



Dynamic Analysis of Continuous Pin Insertion Machines and Their Application in Precision Connector Manufacturing

Yi Du^{*}

School of Electronic Information and Electrical Engineering, Anyang Institute of Technology, 455000 Anyang, China

^{*} Correspondence: Yi Du (20170020@ayit.edu.cn)**Received:** 08-05-2024**Revised:** 09-18-2024**Accepted:** 09-24-2024

Citation: Y. Du, "Dynamic analysis of continuous pin insertion machines and their application in precision connector manufacturing," *Precis. Mech. Digit. Fabr.*, vol. 1, no. 3, pp. 158–175, 2024. <https://doi.org/10.56578/pmdf010304>.



© 2024 by the author(s). Published by Acadlore Publishing Services Limited, Hong Kong. This article is available for free download and can be reused and cited, provided that the original published version is credited, under the CC BY 4.0 license.

Abstract: In the production of high-precision electronic connectors, the proper alignment and insertion quality of pins are critical to ensuring product reliability. Any pin misalignment or deformation can lead to electrical failures in connectors, such as poor contact or pin breakage. To address this issue, this paper conducts a systematic dynamic analysis of the pin insertion mechanism in continuous pin insertion machines, aiming to minimize defects during production and inspection processes. The study first outlines the working principles of continuous pin insertion machines and provides a comprehensive analysis of the pin insertion mechanism, control system, and visual inspection system. By establishing a dynamic model of the pin insertion mechanism, the research uses Matlab for simulation to explore the effects of clearance values, motor speeds, and different materials on the dynamic characteristics of the pin bar. Additionally, a comprehensive test platform was constructed, comprising a feeding module, pinhead, servo worktable, pressure sensor, infrared displacement sensor, and an industrial control computer. The experimental results confirm the accuracy of the simulations and reveal specific trends regarding how clearance values, motor driving speeds, and material selection impact the dynamics of the pin bar. The findings of this study not only enhance the operational stability of continuous pin insertion machines but also provide scientific guidance for quality control and defect prevention in precision connector manufacturing.

Keywords: Continuous pin insertion machine; Dynamic analysis; Transient stress analysis

1 Introduction

Precision connectors are essential components in electronic devices, not only providing electrical connections but also promoting the development of specialization, modularization, miniaturization, and high-density production of complete systems. With continuous technological advancements and the trend towards high automation and multifunctionality in electronic devices, the application of precision connectors has expanded, and their usage has increased accordingly [1]. In this process, continuous pin insertion machines, as key equipment for inserting precision connectors into Printed Circuit Boards (PCBs) and plastic parts, directly influence the production outcome and cost-effectiveness of connectors. The working principle of continuous pin insertion machines involves using an electric motor to drive the rotation of the main shaft, which then actuates the pin insertion mechanism through a cam system to perform precise vertical movements. By accurately inserting pins into circuit boards, these machines establish electrical connections, eliminating the need for traditional soldering processes and significantly improving production efficiency [2]. At present, leading global manufacturers of precision connectors have invested substantial resources in enhancing the efficiency and precision of pin insertion machines [3].

However, during the operation of continuous pin insertion machines, issues such as wear in the pin insertion mechanism and unreasonable clearance values often negatively affect the defect detection system and the overall inspection efficiency. Improper clearance can result in significant mechanical errors, making it easier for product failures to occur during the insertion process and indirectly reducing the production efficiency of connectors. Therefore, the precision and reliability of the pin insertion mechanism are crucial factors in improving production efficiency. In continuous pin insertion machines, the clearance in the mechanism's hinges plays a significant role in the reliability of the mechanism's movement and the frictional deformation during the pin insertion process.

The objective of this study is to design the structure of continuous pin insertion machines and analyze their working principles. Focusing on the issues in the pin insertion mechanism, this paper establishes a dynamic model for

the pin insertion mechanism and conducts simulation analysis using Matlab programming. It thoroughly investigates the impact of the clearance values in the kinematic pairs, motor driving speed, and different materials on the dynamic characteristics of the pin bar. The research includes an analysis of the effects of clearance values, speeds, and material properties on the dynamic characteristics of the pin bar. Through these analyses, this study not only deepens the understanding of the dynamic characteristics of continuous pin insertion machines but also provides a theoretical basis for optimizing their design. Finally, experimental tests were conducted to verify the accuracy of the simulation analysis, ensuring consistency between theory and practice, thereby enhancing the performance and reliability of continuous pin insertion machines in engineering applications.

2 Theoretical Background

2.1 Current Research on the Dynamics of Mechanisms with Clearance

Extensive research has been conducted both domestically and internationally on the dynamics of mechanisms with clearance. Ding et al. [4] studied the dynamic characteristics of rigid-body mechanisms with clearance. Erkaya and Uzmay [5] investigated the positioning errors in hinge mechanisms with clearance and analyzed the motion sensitivity and positioning accuracy. Schwab et al. [6] explored the influence of clearance and rod elastic deformation on the dynamic performance of crank-slider mechanisms, using continuous and discontinuous contact-collision force models. Muvengei et al. [7], based on the L-N model, analyzed the impact of input speed and hinge location on the dynamic characteristics of mechanisms, assuming the absence of tangential friction at the clearance joints. Pereira et al. [8] developed a contact-collision force model for crank-slider mechanisms with clearance and examined the effects of small clearances and high loads. Their study pointed out the limitations of existing collision force models and showed that purely elastic contact models, which neglect energy dissipation, can result in significant discrepancies between simulation and real-world outcomes. Khemili and Romdhane [9] combined numerical simulation with experimental validation to analyze the dynamic characteristics of clearance mechanisms in both multi-body and rigid-flexible coupled systems. Jing et al. [10] used ANSYS software and finite element simulations to analyze the influence of geometric parameters on the performance of design models and optimized these parameters using multi-criteria decision models.

In China, Wang et al. [11] examined the effects of nonlinear factors on the dynamic performance of linkages. Xue [12] from Xi'an University of Technology analyzed the influence of clearance size, crank speed, material properties, and clearance location on the dynamic performance of mechanisms, using Hertz theory and elastic foundation models. Kaitwanidvilai et al. [13] proposed an algorithm based on wavelet transformation to detect chip pin count defects by extracting characteristic information from the chip pins. Bergès et al. [14] applied image processing techniques to inspect MOSFET packaged chips, detecting the number of pinholes by comparing the contrast differences between metal and pinhole areas in the images. Saad et al. [15] introduced an automated defect segmentation algorithm for semiconductor wafer images using multi-thresholding. Their method converts RGB images to grayscale, applies median filtering for enhancement, and implements an improved multi-threshold algorithm to accurately segment defects, outperforming other thresholding techniques. Perminov et al. [16] proposed an automated image processing method to detect wafer chip defects by calculating the shape and dimensions of dies based on edge displacements along the die paths. Gaidhane et al. [17] developed a similarity measurement algorithm to detect surface defects on PCB chips effectively. Ryu et al. [18] introduced a feature-based inspection method, which enhances pin connector defect detection by incorporating new process-sensitive features without requiring improved hardware performance. Wright and Yang [19] trained a RetinaNet convolutional neural network to automatically extract regions of interest (ROIs) from SEM wafer images, achieving faster ROI extraction [19, 20].

2.2 Current Research on the Dynamics of Continuous Mechanisms

The dynamics of multi-body systems have been widely applied in fields such as aerospace and automotive engineering, and after decades of effort by scientists, the technology has matured. However, progress in flexible multi-body system dynamics has been slower due to the challenges of understanding and handling the coupling between large-scale motion and elastic deformation [21].

One branch of dynamic research that considers component elasticity is mechanism elastic dynamics. This approach does not account for the influence of elastic deformation on large-scale motion but instead analyzes the kinematic behavior of components using multi-body system dynamics. The inertia properties of components are included as inertial forces, which are then used in combination with external forces to analyze elastic deformation and strength. However, the rise of modern lightweight, high-speed mechanical systems has highlighted the limitations of mechanism elastic dynamics. To address the effect of deformation on large-scale motion, the hybrid coordinate method was developed. This method assumes that the configuration of a component is the superposition of large-scale motion in a floating coordinate system and deformation relative to that system. However, it only accounts for elastic deformation, and by introducing a floating coordinate system, it models deformation as the sum of several linear fields. As a result, the model size remains relatively small. However, the component mode synthesis (CMS) method

faces difficulties in handling non-linear problems, unlike non-linear finite element analysis (FEA), which can consider arbitrary material and geometric non-linearities. Furthermore, the component modes used are fixed at a certain moment, meaning that potential changes in modal characteristics during motion are not accounted for. Despite these limitations, research over the years has shown that the results of flexible multi-body dynamics analysis using the CMS method align closely with many real-world engineering scenarios, particularly when the large-scale motion speed of components is relatively low [22].

2.3 Problem Analysis of the Pin Insertion Mechanism

The pin insertion mechanism is modeled using SolidWorks, where the main shaft serves as the transmission element, and the cutting mechanism operates after continuous pin cutting, followed by the insertion process executed by the insertion mechanism. During the manufacturing of precision connector products, the insertion mechanism plays a crucial role. However, the insertion mechanism introduces clearances, leading to two states of relative motion that switch during operation. Upon re-engagement, mechanical collisions occur. In high-speed mechanical systems, variables such as acceleration, interaction forces, and balancing torques resulting from mechanical contact and collisions may exceed the rated values, significantly impacting pin insertion operations.

3 Modeling and Simulation Methods

The insertion mechanism plays a central role in the pin insertion process, as shown in Figure 1. To meet operational requirements, the dynamics of mechanisms with clearance must be analyzed. The introduction of clearances creates two states of relative motion, which transition back and forth between free movement and contact collisions. These collisions can impact the stability of the insertion mechanism.

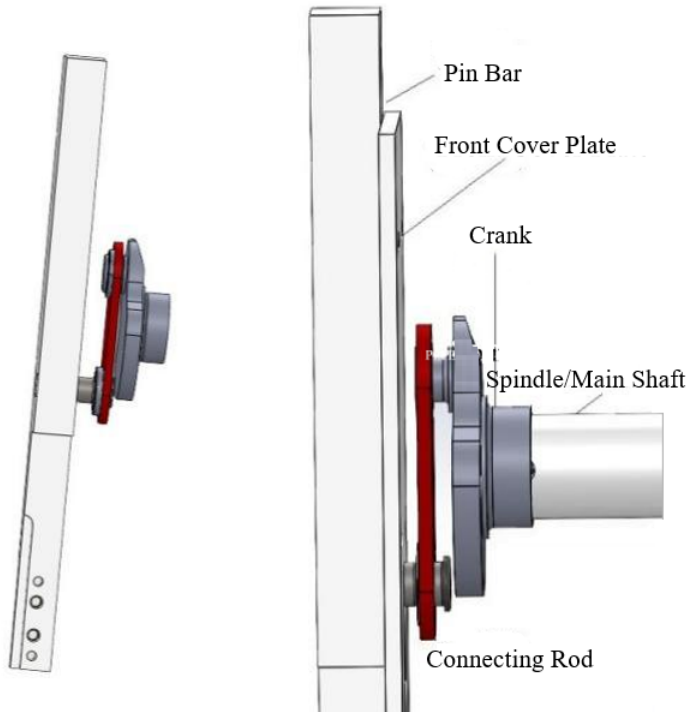


Figure 1. Insertion mechanism

3.1 Establishment of the Dynamic Model for the Pin Insertion Mechanism

When the kinematic pairs within the pin insertion mechanism contain clearance, the transition between free motion and contact collision occurs during operation. This study uses the Lagrange multiplier method to develop the dynamic equations of hinge mechanisms with clearance. Below is the construction of the dynamic model for the insertion mechanism:

$$\begin{cases} M\ddot{x} + C\dot{x} + Kx + \phi^T \lambda = F + F_C \\ \phi(x, t) = 0 \end{cases} \quad (1)$$

In the equation, the parameter M represents the generalized mass matrix, C represents the generalized damping matrix, and K represents the generalized stiffness matrix. The parameter x denotes the generalized coordinate vector, and φ represents the Jacobian matrix of the constraint equations. The parameter λ is the Lagrange multiplier vector. F and F_C represent the generalized force vector and collision force vector, respectively. The collision force vector F_C consists of the normal collision force F_N and the tangential friction force F_T .

$$F_C = \mu(\delta) (F_N + F_T) \quad (2)$$

where, $\mu(\delta)$ is the unit step function:

$$\mu(\delta) = \begin{cases} 0, & \delta < 0 \\ 1, & \delta \geq 0 \end{cases} \quad (3)$$

where, when $\mu(\delta) = 0$, that is, $\delta = e - c = 0$. This moment corresponds to the transition between the free state and the collision state, which is difficult to obtain an exact solution for in numerical calculations. A numerical approximation is used to solve it, gradually reducing the integration step size until the corresponding switching point is reached.

$$|e - c| < \varepsilon \quad (4)$$

where, ε is the integration error, with a value no greater than 10^{-5} .

3.2 Analysis of the Pin Insertion Mechanism Model

As shown in subgraph (a) of Figure 2, a simplified model of the pin insertion mechanism is presented, followed by assumptions about its motion state: all components used are rigid bodies; the kinematic pairs are ideal connections without lubrication; the angular speed and initial speed during crank motion are both zero; during the analysis, only system inertia and collisions are considered, while the working resistance of the slider is neglected.

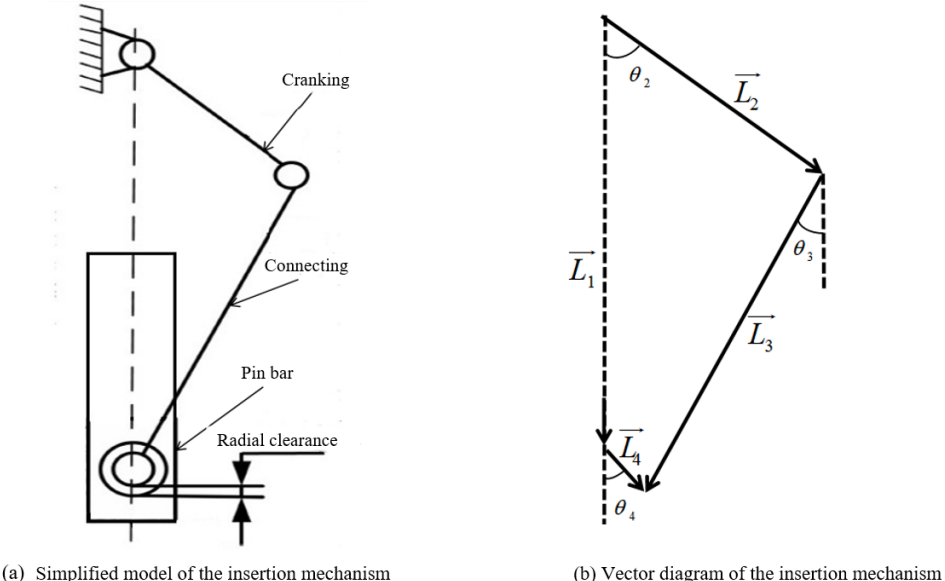


Figure 2. Insertion mechanism model

The displacement of the pin bar is denoted by L_1 , while the scalars of the crank and connecting rod are represented by L_2 and L_3 , respectively. L_4 denotes the offset between the element shaft and the center of the bearing. θ_2 and θ_3 are the angles between the crank and the connecting rod with the ground, respectively, and θ_4 is the angle between the offset of the shaft and the bearing center with the ground. This paper applies the dynamic-static analysis method for modeling, assuming the main shaft rotates at a constant speed. According to the diagram shown in subgraph (b) of Figure 2, the kinematic vector equation can be derived as:

$$\vec{L}_2 + \vec{L}_3 + \vec{L}_4 = \vec{L}_1 \quad (5)$$

Projecting Eq. (5) along the x -axis and y -axis yields the following scalar equations:

$$L_2 \cos \theta_2 + L_3 \cos \theta_3 + L_4 \cos \theta_4 = L_1 \quad (6)$$

$$L_2 \sin \theta_2 + L_3 \sin \theta_3 + L_4 \sin \theta_4 = 0 \quad (7)$$

Taking the second derivative of Eqs. (6) and (7) with respect to time yields:

$$\begin{aligned} & -\ddot{L}_1 - \ddot{L}_4 \cos \theta_4 - L_3 \sin \theta_3 \alpha_3 - L_4 \sin \theta_4 \alpha_4 \\ & = L_2 \cos \theta_2 \omega_2^2 + L_3 \cos \theta_3 \omega_3^2 + 2\dot{L}_4 \sin \theta_4 \omega_4 + L_4 \cos \theta_4 \omega_4^2 \end{aligned} \quad (8)$$

$$\begin{aligned} & \ddot{L}_4 \sin \theta_4 + L_4 \cos \theta_4 \alpha_4 + L_3 \cos \theta_3 \alpha_3 \\ & = L_2 \sin \theta_2 \omega_2^2 - 2\dot{L}_4 \cos \theta_4 \omega_4 + L_2 \sin \theta_2 \omega_2^2 + L_3 \sin \theta_3 \omega_3^2 \end{aligned} \quad (9)$$

The coordinates of the crank's centroid are given by:

$$\begin{aligned} x_{c2} &= L_{c2} \cos \theta_2 \\ y_{c2} &= L_{c2} \sin \theta_2 \end{aligned} \quad (10)$$

Taking the second derivative of Eq. (10) with respect to time provides the horizontal and vertical accelerations of the crank's centroid:

$$\begin{aligned} a_{c2x} &= -L_{c2} \cos \theta_2 \omega_2^2 \\ a_{c2y} &= -L_{c2} \sin \theta_2 \omega_2^2 \end{aligned} \quad (11)$$

Similarly, the coordinates of the connecting rod's centroid are:

$$\begin{aligned} x_{c3} &= L_2 \cos \theta_2 + L_4 \cos \theta_4 + L_{c3} \cos \theta_3 \\ y_{c3} &= L_2 \sin \theta_2 + L_4 \sin \theta_4 - L_{c3} \sin \theta_3 \end{aligned} \quad (12)$$

The second derivatives of Eq. (12) yield the horizontal and vertical accelerations of the connecting rod's centroid:

$$\begin{aligned} & a_{c3x} - \ddot{L}_4 \cos \theta_4 + L_4 \sin \theta_4 \alpha_4 + L_{c3} \sin \theta_3 \alpha_3 \\ & = -L_2 \cos \theta_2 \omega_2^2 - 2\dot{L}_4 \sin \theta_4 \omega_4 - L_4 \cos \theta_4 \omega_4^2 - L_{c3} \cos \theta_3 \omega_3^2 \end{aligned} \quad (13)$$

$$\begin{aligned} & a_{c3y} - \ddot{L}_4 \sin \theta_4 - L_4 \cos \theta_4 \alpha_4 + L_{c3} \cos \theta_3 \alpha_3 \\ & = -L_2 \sin \theta_2 \omega_2^2 + 2\dot{L}_4 \cos \theta_4 \omega_4 - L_4 \sin \theta_4 \omega_4^2 + L_{c3} \sin \theta_3 \omega_3^2 \end{aligned} \quad (14)$$

In the above equations, ω_i represents the angular speed corresponding to the angle θ_i ; α_i represents the angular acceleration of the corresponding angle θ_i ; L denotes the acceleration corresponding to L_i ; and L_{ci} denotes the distance from the center of mass to the vertex.

The dynamic equilibrium equations of forces and torques for the crank, connecting rod, and pin bar can be expressed as the following expressions:

$$\left\{ \begin{array}{l} F_{i(i+1)x} + F_{(i+2)(i+1)x} = m_{(i+1)} \ddot{x}_{G(i+1)} \\ F_{i(i+1)y} + F_{(i+2)(i+1)y} = m_{(i+1)} g + m_{(i+1)} \ddot{y}_{G(i+1)} \\ \sum M_{G(i+1)} = I_{G(i+1)} \ddot{\theta}_{G(i+1)} \end{array} \right. \quad (15)$$

In the equations, $F_{i(i+1)x}$ and $F_{i(i+1)y}$ represent the forces of the kinematic pair elements i and $i + 1$ in the x - and y -axis directions, respectively.

From Figure 3, M_{12} represents the balanced external moment. The force and moment balance of the crank are as follows:

$$\begin{aligned}
F_{12x} - F_{32x} + m_2 a_{2x} &= 0 \\
F_{12y} - F_{32y} - m_2 a_{2y} &= m_2 g \\
F_{12x} L_{c2} \sin \theta_2 - F_{12y} L_{c2} \cos \theta_2 - F_{32x} L_{c2} \sin \theta_2 + F_{32y} L_{c2} \cos \theta_2 &= M_{12}
\end{aligned} \tag{16}$$

From Figure 4, the force and moment balance of the connecting rod are as follows:

$$\begin{aligned}
F_{32x} + F_{43x} + m_3 a_{c3x} &= 0 \\
- F_{32y} - F_{43y} + m_3 a_{c3y} &= m_3 g \\
- F_{32x} [(L_3 - L_{c3}) \sin \theta_3 + L_4 \sin \theta_4] + F_{32y} [(L_3 - L_{c3}) \cos \theta_3 + L_4 \cos \theta_4] \\
+ F_{43x} L_{c3} \sin \theta_3 - F_{43y} L_{c3} \cos \theta_3 - I_3 \alpha_3 &= 0
\end{aligned} \tag{17}$$

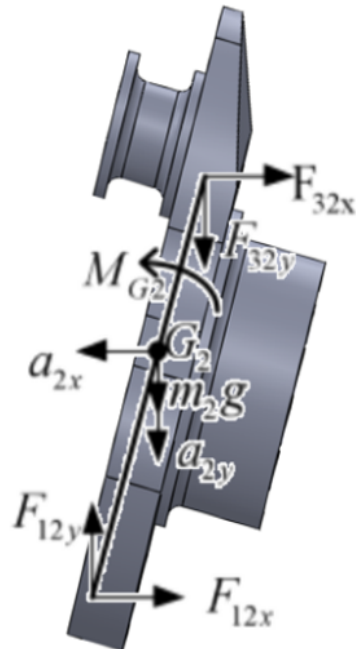


Figure 3. Crank force analysis

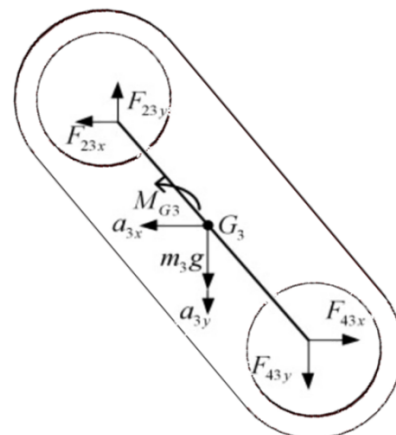


Figure 4. Connecting rod force analysis

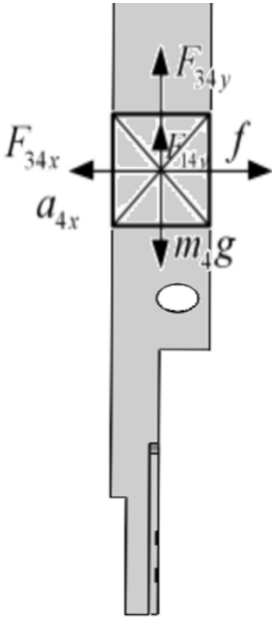


Figure 5. Pin bar force analysis

From Figure 5, the force balance of the pin bar is as follows:

$$\begin{aligned} F_{34y} + F_{14y} &= m_4g \\ f - F_{34x} - m_4\ddot{L}_1 &= 0 \end{aligned} \quad (18)$$

The stability of the pin insertion mechanism will be studied below, focusing mainly on the effects of the clearance size between the connecting rod and the pin bar, the driving speed of the prime mover, and material properties on the motion performance of the pin bar within the mechanism.

4 Simulation Results and Analysis

Using the previously derived dynamic equations for the insertion mechanism with clearance, a simulation program was developed in MATLAB. This allows for solving the equations at any given time step and generating simulation data. Once the system reaches steady-state conditions, the periodic behavior of the mechanism can be analyzed. Since the dynamic equations include ordinary differential equations (ODEs), the Runge-Kutta method was chosen for numerical integration due to its high accuracy. With the given initial conditions, no additional methods were needed for the simulation process. The key parameters used for the simulation are listed in Table 1.

Table 1. Simulation analysis parameters

Parameter	Value
Max integration step	10^{-5} s
Integration error	10^{-6}
Young's modulus (GPa)	Stainless steel (190), Tungsten steel (344.7), Copper (120)
Poisson's ratio	Alloy steel (0.3), Aluminum (0.33), Stainless steel (0.305), Tungsten steel (0.28), Copper (0.326)
Bearing radius (mm)	7.5
Bearing width (mm)	10
Spindle speed (rpm)	1000, 1200, 1500, 1800, 2000
Clearance size (mm)	0, 0.1, 0.3, 0.5, 0.8

4.1 Analysis of the Impact of Clearance Value on the Dynamic Characteristics of the Pin Bar

According to the requirements of the continuous pin insertion machine's pin insertion operation, assuming a motor-driven speed of 1200 rpm and a friction coefficient of 0.01 between the pin bar and the front cover plate of the pin head, all components of the mechanism are made of alloy steel. The clearance values between the pin bar's moving

shaft and the connecting rod bearing are set at 0.1 mm, 0.3 mm, 0.5 mm, and 0.8 mm. The following are comparative graphs of the displacement, speed, acceleration, and motor torque of the pin bar against the ideal curve ($c=0$).

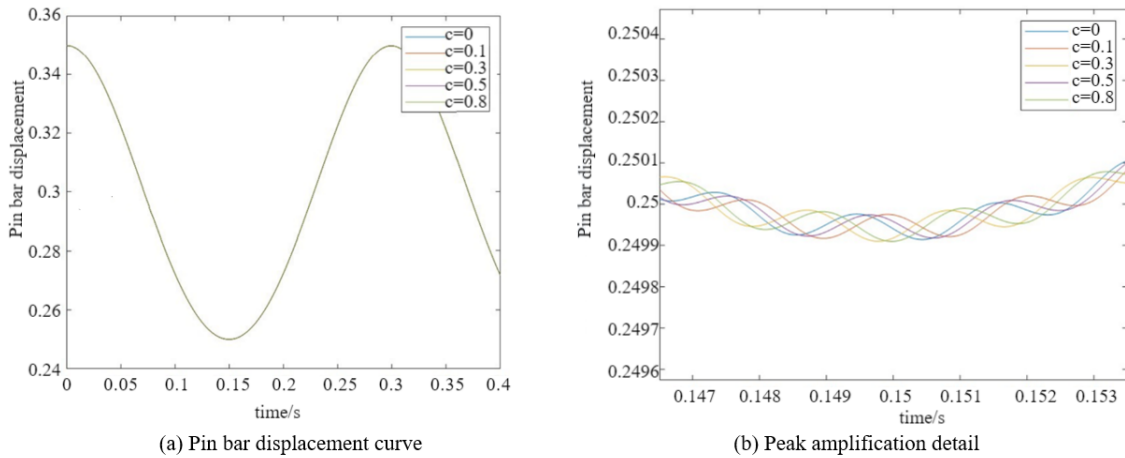


Figure 6. Displacement diagram of pin bar in different clearance

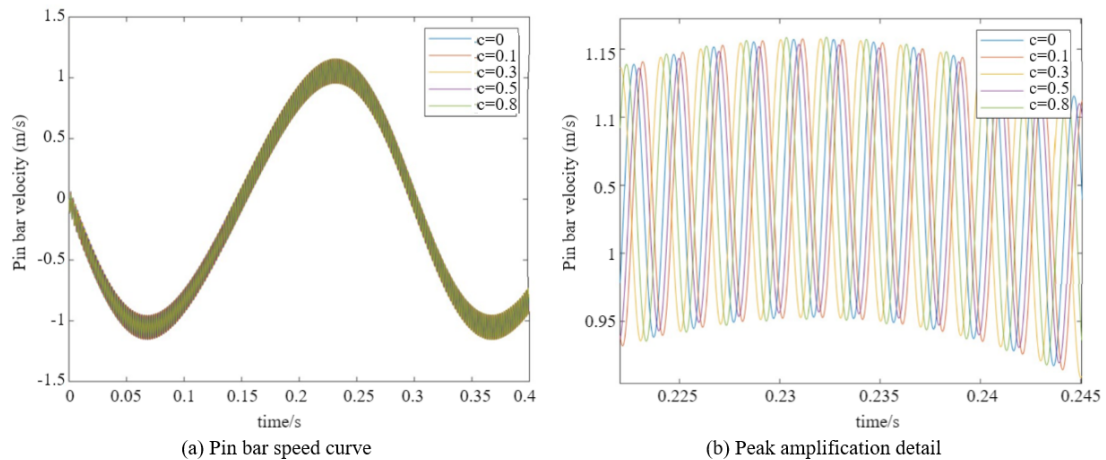


Figure 7. Speed chart of pin bar at different clearance

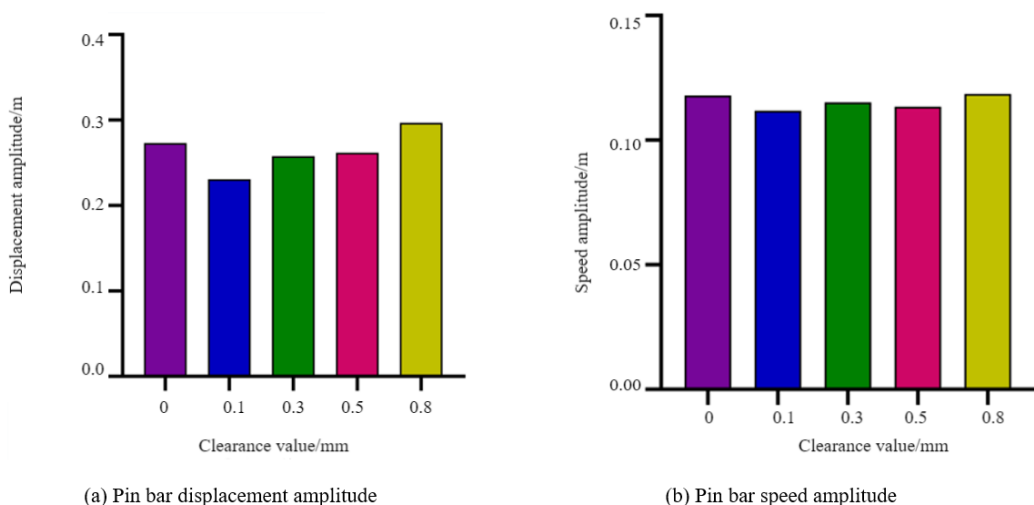


Figure 8. Histogram of amplitude at different clearance values

From Figure 6, the insertion cycle of the pin insertion mechanism is approximately 0.3 s. The displacement curve of the pin bar indicates that the size of the clearance between different kinematic pairs has a minor effect on the displacement of the pin bar. However, when used in high-speed and high-precision machines, where positional accuracy is critical, the clearance values between the kinematic elements cannot be overlooked.

Similarly, from Figure 7, the speed curve of the pin bar shows that different clearance sizes between the kinematic pairs have a minimal impact on the speed of the pin bar, and overall, no significant fluctuations are observed. As the clearance value increases, the minimum film thickness gradually decreases, with the lowest values occurring near the pole position.

From the graphs of displacement and speed of the pin bar under different clearance values, as shown in Figure 8, when the clearance value between the connecting rod motion pair is 0.1 mm, the displacement and speed amplitudes of the pin bar are minimal. This indicates that, compared to other clearance values, the pin bar operates more stably at this value during the insertion work.

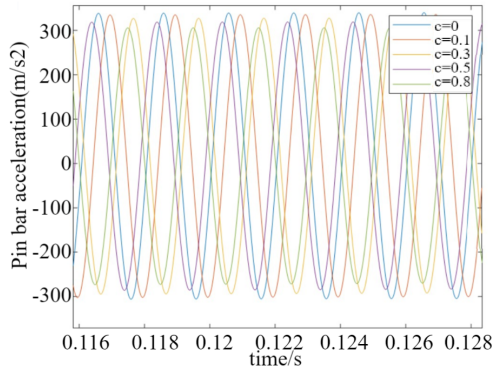


Figure 9. Acceleration curves of the pin bar at different clearances

From the acceleration change curve shown in Figure 9, it can be observed that the clearance has a minimal effect on the acceleration of the pin bar. Due to the small fluctuations in the peak amplitude of the acceleration curve, as the clearance value increases, the amplitude of the acceleration gradually deviates from the ideal curve. This not only reflects the rate of change of the pin bar's speed but also indicates that as the clearance value increases, the fluctuations during the operation of the pin bar become more pronounced, severely affecting the stability of the pin insertion mechanism.

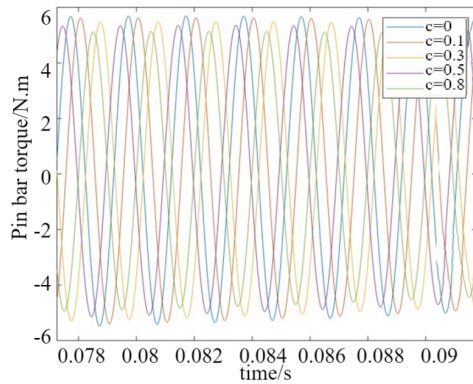


Figure 10. Torque curve of pin bar at different clearances

From the torque variation curve of the pin bar under different clearances shown in Figure 10, it can be observed that as the clearance value increases, the deviation of the main shaft torque from the ideal curve also increases. This indicates that as the clearance value increases, the external balancing torque required for the pin bar becomes increasingly unstable. Therefore, the increase in clearance values will exacerbate the impact of vibrations and shocks on the insertion mechanism.

4.2 Analysis of Speed's Impact on Pin bar Dynamic Characteristics

Assuming the clearance value of the connecting rod motion pair is 0.1 mm, with a friction coefficient of 0.01 during the downward movement of the pin bar, and that the materials of the insertion mechanism components are also

alloy steel, the motor driving speeds are set at 1000 rpm, 1200 rpm, 1500 rpm, 1800 rpm, and 2000 rpm.

From the displacement and speed of the pin bar at different driving speeds, as shown in Figure 11 and Figure 12, it can be observed that as the driving speed increases, the fluctuations of the pin bar's displacement and speed also increase, assuming no friction and deformation of the parts are considered during the simulation process. If we compare the average deviation of the displacement and speed fluctuations of the pin bar within the same cycle, as illustrated in subgraph (b) of Figure 11 and subgraph (b) of Figure 12, the fluctuation amplitude of the pin bar is minimal when the motor driving speed is 1200 rpm.

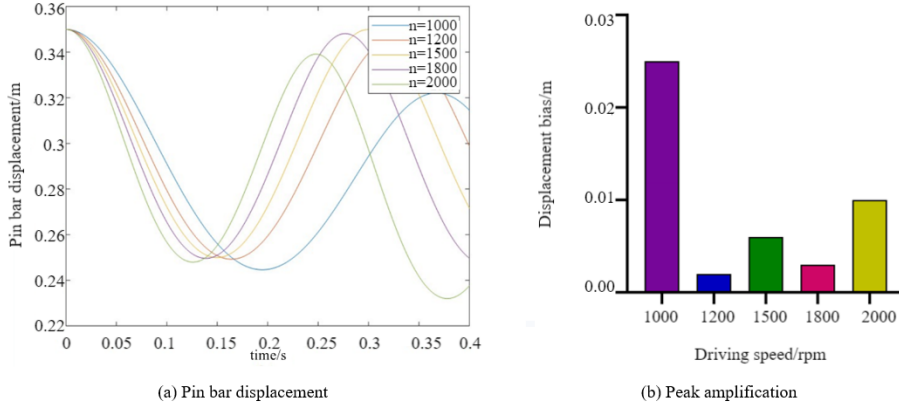


Figure 11. Displacement curve of pin bar under different drives

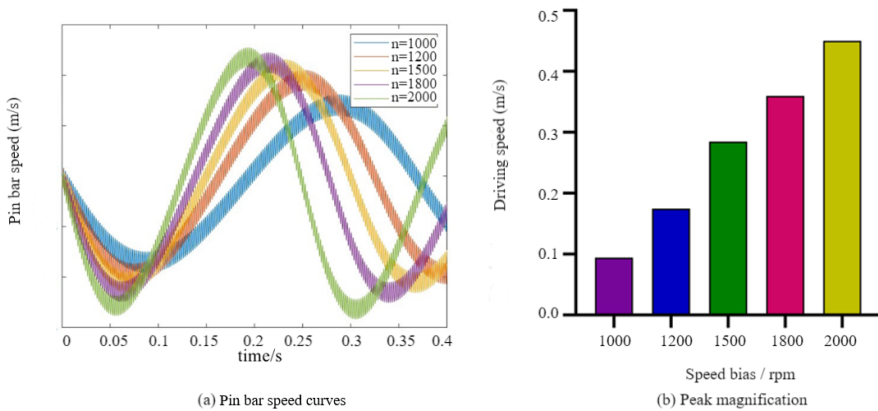


Figure 12. Speed profile of the pin bar under different drives

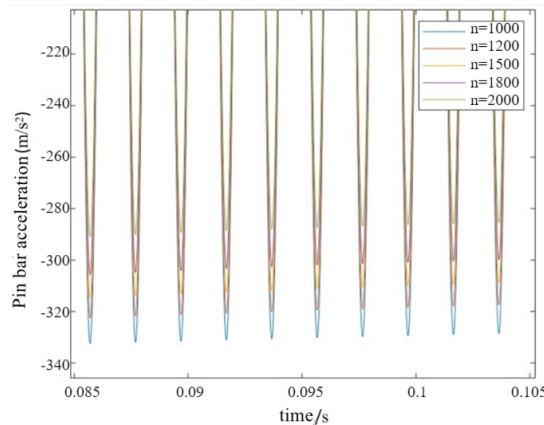


Figure 13. Acceleration curves of the pin bar under different drives

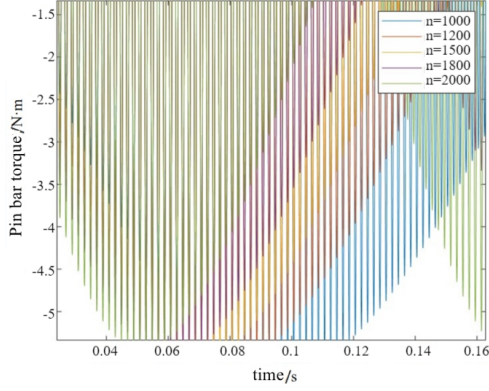


Figure 14. Torque curve of the pin bar under different drives

From the analysis of Figure 13, it can be seen that for a clearance value of 0.1 mm, the corresponding peak acceleration values of the pin bar at driving speeds of 1000 rpm, 1200 rpm, 1500 rpm, 1800 rpm, and 2000 rpm are 290.24 m/s^2 , 303.25 m/s^2 , 316.28 m/s^2 , 322.51 m/s^2 , and 336.21 m/s^2 , respectively. From the comparison of the data, it is evident that as the speed increases, the difference in peak acceleration remains unchanged, indicating that at a clearance value of 0.1 mm, the motor driving speed has little effect on the pin bar's acceleration.

From Figure 14, it can be observed that as the motor driving speed increases, the torque experienced by the pin bar shows increased oscillation, and the greater the speed, the larger the oscillation peaks. This indicates that as the speed increases, the torque changes more rapidly and becomes less stable. Therefore, for mechanisms operating at high speeds, special attention should be paid to the effects of clearance.

From the displacement and speed amplitudes of the pin bar under different driving speeds, as shown in Figure 15, when the motor driving speed is 1200 rpm, the displacement amplitude and speed amplitude of the pin bar are the smallest, indicating that compared to other driving speeds, the pin bar is more stable during the pin insertion work.

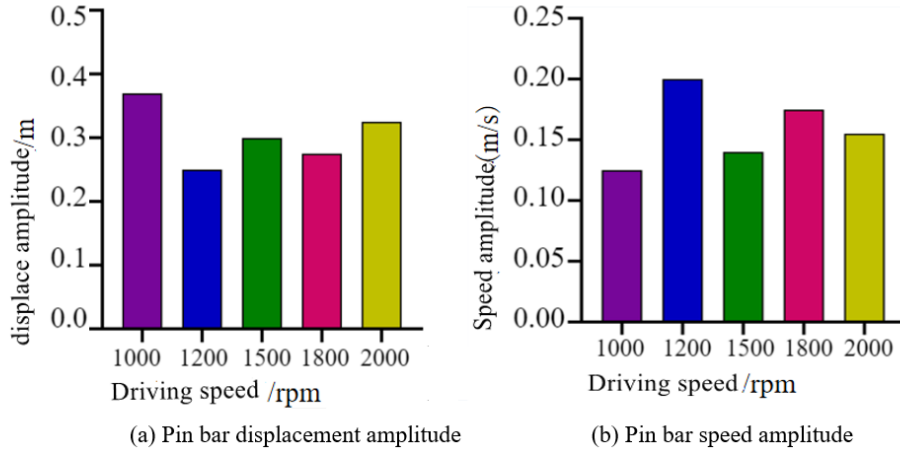


Figure 15. Histogram of amplitude at different driving speeds

4.3 Analysis of Material Properties on the Dynamic Characteristics of the Pin Bar

Assuming that the motor driving speed is 1200 rpm, the friction coefficient between the pin bar and the ground is set to 0.01, and the clearance value between the motion pair shaft and the bearing is 0.1 mm, while neglecting component deformation and friction during the simulation process, the selected combination of material types for the insertion mechanism includes alloy steel, aluminum, stainless steel, tungsten steel, and copper, using the Young's modulus of each material for comparison.

The following are the displacement, speed, acceleration, and torque curves of the pin bar, as shown in Figure 16. The influence patterns of acceleration and pin bar torque are similar. From the performance of the insertion mechanism, it can be observed that the curves of the pin bar nearly coincide, indicating that the effect of different material combinations on the acceleration and torque of the pin bar is minimal, while their effect on the displacement and speed of the pin bar is significant.

The different material combinations mainly change the equivalent contact stiffness in the model, and the greater the ratio of different material combinations, the more it seems to mitigate impact collisions. Under different materials, as shown in Figure 17, when the Young's modulus of the selected combination material for the insertion mechanism is 207, which is alloy steel, the amplitude of the displacement and speed deviations of the pin bar is the smallest, indicating that compared to other materials, using alloy steel makes the pin bar more stable during pin insertion work.

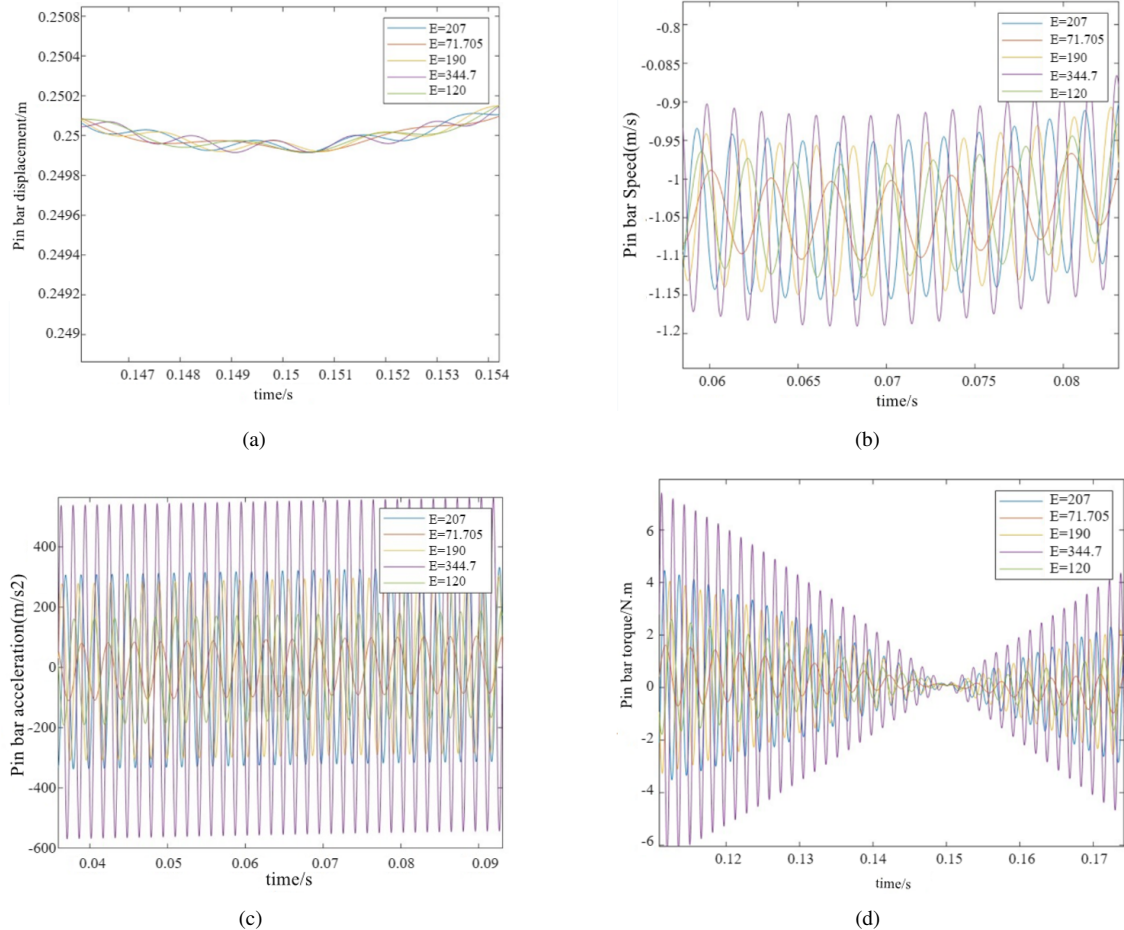


Figure 16. Curves of pin bar in case of different materials: (a) Displacement; (b) Speed; (c) Acceleration; (d) Torque

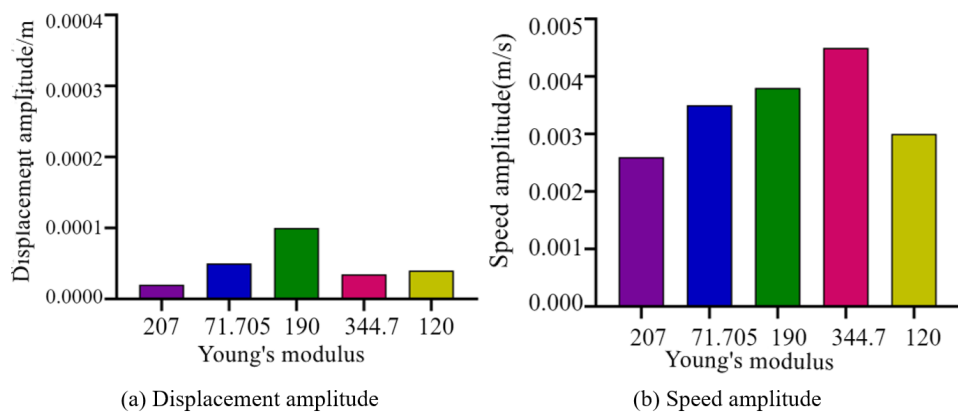


Figure 17. Histogram of amplitude with different materials

5 Experimental Verification

To investigate the stability of the continuous pin insertion machine, an experimental setup for the assembly process of the continuous pin insertion machine was constructed, as shown in Figure 18 and Figure 19. This experimental setup mainly consists of a feeding module, pin insertion head, servo workbench, pressure sensor, infrared displacement sensor, and industrial computer.

First, the continuous pins were taken and placed into the feeding module. Then, plastic parts were properly positioned in the tooling. Through the user interface of the industrial control platform, different insertion speeds (1000 rpm, 1200 rpm, 1500 rpm, 1800 rpm, and 2000 rpm) were set for the assembly operation. Finally, the insertion force and displacement of the pins were measured using the pressure sensor and laser displacement sensor to observe the variation of insertion force and displacement within a certain range.

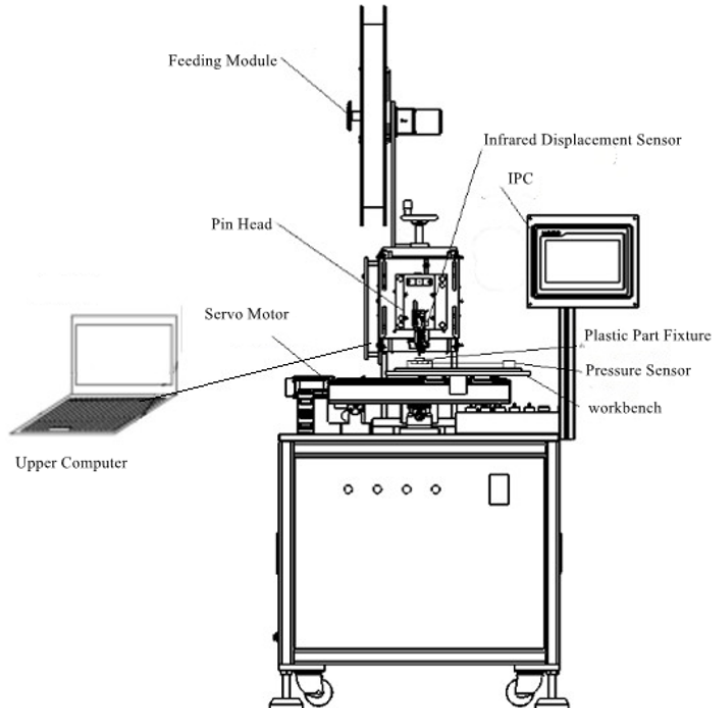


Figure 18. Experimental schematic diagram



Figure 19. Experimental setup photo

5.1 Experimental Result Analysis

Before performing the assembly operation, it is necessary to set the corresponding rotational speed in the program editing interface. Under the premise that the pin insertion head is positioned directly above the plastic part, the distance between the pin insertion head and the plastic part must be equal before each assembly. The pin insertion test process is shown in Figure 20.

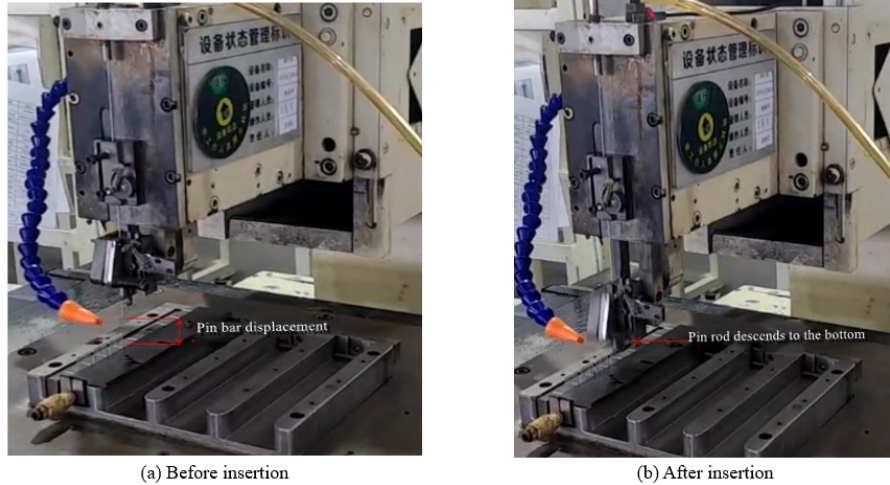


Figure 20. Assembly experiment process

The pressure sensor is zeroed. When the pin is inserted into the plastic part, the value displayed by the pressure sensor represents the insertion and withdrawal force of the pin during the assembly of the continuous pin insertion machine. From Figure 21, we can observe that as the spindle speed increases, the values of the insertion and withdrawal force of the pin fluctuate correspondingly, indicating that with the increase of the motor drive, the inertial force becomes more significant, making the pin insertion mechanism increasingly unstable, especially noticeable when the speed exceeds 1200 rpm.

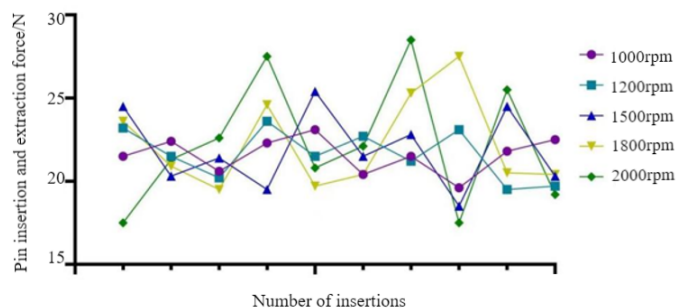


Figure 21. Insertion and extraction force test

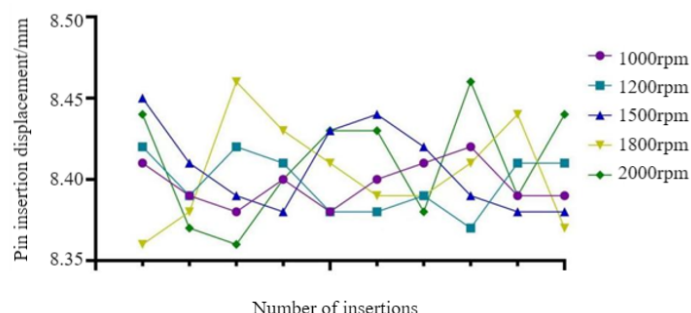


Figure 22. Insertion displacement test

The laser displacement sensor is also zeroed. When the spindle operates, the value displayed by the displacement sensor represents the distance the pin bar descends from the pin to the plastic part. From Figure 22, we can see that as the spindle speed increases, the fluctuation in the insertion displacement value correspondingly increases, indicating that with the increase in motor drive, there may be a misalignment of the pin with the precision connector.

Based on the average values of the pin insertion and extraction force and the insertion displacement amplitude, as shown in Figure 23, we can see that at a speed of 1200 rpm, the insertion and extraction force is closer to the actual working value of 21 N, and the displacement amplitude of the pin bar has the smallest deviation, indicating the most stable operation.

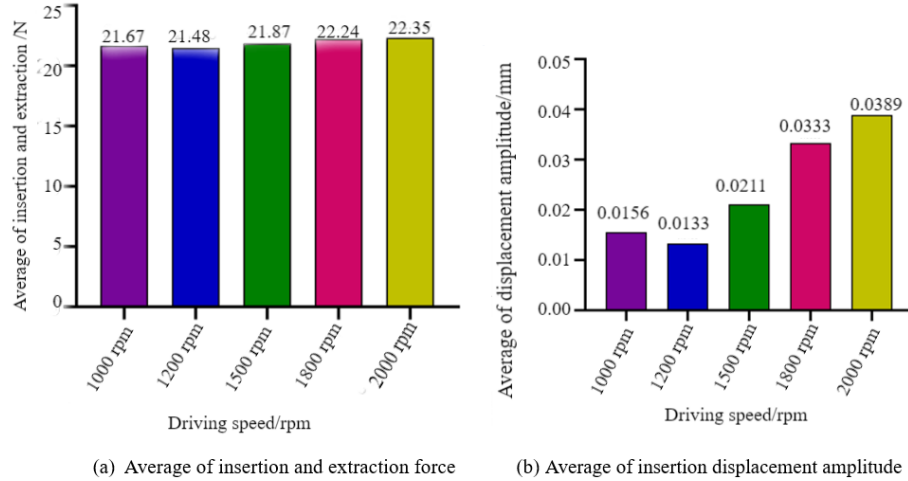


Figure 23. Histogram of mean values

6 Insertion Mechanism Stability Experiment

6.1 Principle of Insertion Mechanism Stability Experiment

In this experiment, the fit tolerances and surface roughness between the crank, connecting rod, and pin bar were strictly controlled. During the experiment, all three joints were lubricated with grease. Additionally, different radial clearances were designed at the connection rotation joints of the connecting rod to study the influence of clearance size and motor driving speed on the displacement of the pin bar. Different radial clearances for the connecting rod are shown in Figure 24.

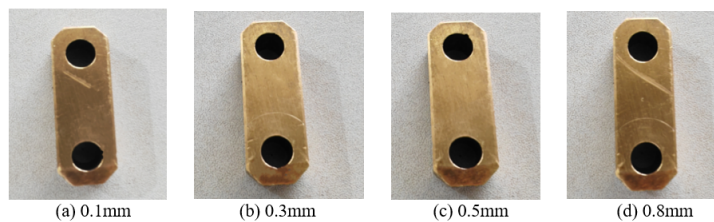


Figure 24. Connecting rods with different radial clearances

6.2 Experimental Result Analysis

The following experimental tests were conducted under conditions of different radial clearances (0.1 mm, 0.3 mm, 0.5 mm, and 0.8 mm) of the connecting rod and different spindle speeds (1000 rpm, 1200 rpm, 1500 rpm, 1800 rpm, and 2000 rpm). The displacement of the pin bar was measured using a displacement sensor, and the obtained test data was processed.

For the displacement experimental results under different radial clearance values of the connecting rod, the results closely resemble the displacement trajectory of the pin bar from the previous simulation. From Figure 25, it can be observed that as the radial clearance of the connecting rod increases, a significant deviation appears between the displacement curve of the pin bar and the ideal curve ($c=0$). This indicates that with the increase in the clearance of the hinge mechanism, the deviation near the extreme position of the mechanism's movement also increases.

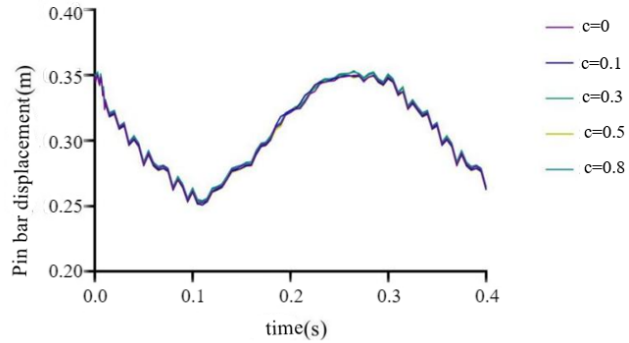


Figure 25. Displacement of pin bar in case of different clearance values

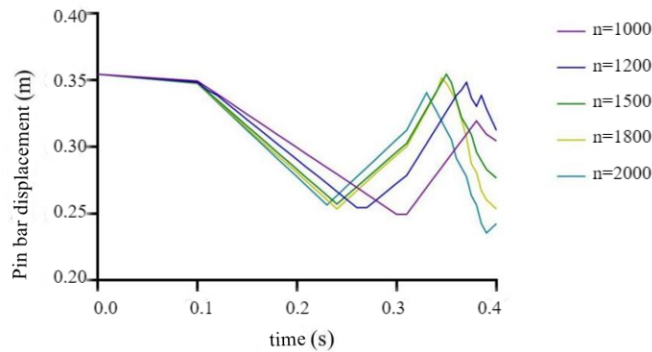


Figure 26. Displacement of the pin bar at different speeds

Similarly, for the displacement experimental results at different speeds, with the clearance set at 0.1 mm, as shown in Figure 26, it is consistent with the simulation results that the displacement fluctuations of the pin bar become more pronounced as the spindle speed increases.

7 Conclusions

This study successfully designed the structure of the continuous pin insertion machine and conducted an in-depth analysis of its working principle. By constructing the dynamic model of the pin insertion mechanism, this paper utilized Matlab for simulation analysis, detailing the impact of connecting rod joint clearance, motor driving speed, and different material combinations on the dynamic characteristics of the pin bar. Further analysis was performed on the working process of the pin insertion mechanism using multi-body dynamics theory, and numerical simulations of the wear condition of the insertion mechanism and the dynamic characteristics of the contact state between the cam and the needle cutting mechanism were conducted using ANSYS software, revealing the transient stress distribution of key components under pin insertion conditions.

The design of experiments (DOE) method was employed for the lightweight design of the pin insertion mechanism, effectively enhancing the lightweight degree of the mechanism while ensuring the pin insertion working requirements, which improved the performance and made the output of the precision connector smoother. Additionally, by creating a prototype of the pin head and building a continuous pin insertion machine experimental platform, this research conducted pin insertion tests for the first time, verifying the effectiveness of the driving parameters by measuring the insertion and withdrawal force and displacement at different driving speeds. Subsequently, by selecting different clearance connecting rods and driving speeds, the stability of the insertion mechanism was successfully verified.

Finally, by establishing a visual inspection experimental platform for precision connectors, the detection yield rate of precision connectors was analyzed. The experimental results were consistent with the simulation analysis, confirming the significant impact of connecting rod joint clearance, motor driving speed, and different material combinations on the dynamic characteristics of the pin bar. These findings not only provide important theoretical and practical support for the design and optimization of the continuous pin insertion machine but also offer technical assistance for the production of precision connectors, enhancing the quality and reliability of the products.

Data Availability

The data used to support the research findings are available from the corresponding author upon request.

Conflicts of Interest

The authors declare no conflict of interest.

References

- [1] Z. F. Bai, F. S. Xu, and J. J. Zhao, “Numerical and experimental study on dynamics of the planar mechanical system considering two revolute clearance joints,” *Int. J. Mech. Syst. Dyn.*, vol. 1, no. 2, pp. 256–266, 2021. <https://doi.org/10.1002/msd2.12022>
- [2] C. N. Wang, T. D. M. Le, and N. T. Huynh, “Optimal rigid-flexible dynamic of space slider-crank mechanism with clearance joints,” *Sādhāraṇā*, vol. 48, p. 44, 2023. <https://doi.org/10.1007/s12046-023-02085-4>
- [3] P. C. Mao, “Research of monitoring system for automatic pin insertion machine,” Ph.D. dissertation, Nanjing University, China, 2018.
- [4] X. L. Ding, Y. Wang, Y. B. Wang, and K. Xu, “A review of structures, verification, and calibration technologies of space robotic systems for on-orbit servicing,” *Sci. China Technol. Sci.*, vol. 64, pp. 462–480, 2021. <https://doi.org/10.1007/s11431-020-1737-4>
- [5] S. Erkaya and I. Uzmay, “Optimization of transmission angle for slider-crank mechanism with joint clearances,” *Struct. Multidisc. Optim.*, vol. 37, pp. 493–508, 2009. <https://doi.org/10.1007/s00158-008-0243-6>
- [6] A. L. Schwab, J. P. Meijaard, and P. Meijers, “A comparison of revolute joint clearance models in the dynamic analysis of rigid and elastic mechanical systems,” *Mech. Mach. Theory*, vol. 37, no. 9, pp. 895–913, 2002. [https://doi.org/10.1016/S0094-114X\(02\)00033-2](https://doi.org/10.1016/S0094-114X(02)00033-2)
- [7] M. Muvengei, J. Kihiu, and B. Ikua, “Effects of clearance size on the dynamic response of planar multi-body systems with differently located frictionless revolute clearance joints,” *J. Energy Technol. Policy*, vol. 2, no. 3, pp. 7–18, 2012.
- [8] C. Pereira, A. Ramalho, and J. Ambrosio, “Applicability domain of internal cylindrical contact force models,” *Mech. Mach. Theory*, vol. 78, pp. 141–157, 2014. <https://doi.org/10.1016/j.mechmachtheory.2014.03.010>
- [9] I. Khemili and L. Romdhane, “Dynamic analysis of a flexible slider-crank mechanism with clearance,” *Eur. J. Mech. A/Solids*, vol. 27, no. 5, pp. 882–898, 2008. <https://doi.org/10.1016/j.euromechsol.2007.12.004>
- [10] Z. L. Jing, L. F. Qiao, H. Pan, Y. S. Yang, and W. J. Chen, “An overview of the configuration and manipulation of soft robotics for on-orbit servicing,” *Sci. China Inf. Sci.*, vol. 60, p. 050201, 2017. <https://doi.org/10.1007/s1432-016-9033-0>
- [11] W. Wang, Z. Shen, Y. L. Song, J. Chen, and S. B. Shi, “Research on system dynamics for linkage mechanism with clearance and dry friction,” *J. Vib. Shock*, vol. 34, no. 18, pp. 210–214, 2015.
- [12] T. Y. Xue, “Dynamic performance and wear analysis of crank-slider mechanism with clearance,” Master’s thesis, Xi’an University of Technology, China, 2022.
- [13] S. Kaitwanidvilai, A. Saenthon, and A. Kunakorn, “Pattern recognition technique for integrated circuit (IC) pins inspection using wavelet transform with chain-code-discrete fourier transform and signal correlation,” *Int. J. Phys. Sci.*, vol. 7, no. 9, pp. 1326–1332, 2012. <https://doi.org/10.5897/IJPS11.1434>
- [14] C. Bergès, P. Soufflet, and A. Jadrani, “Risk and reliability assessment about a manufacturing issue in a power MOSFET for automotive applications,” *Microelectron. Reliab.*, vol. 54, no. 9-10, pp. 1887–1890, 2014. <https://doi.org/10.1016/j.microrel.2014.07.022>
- [15] N. H. Saad, A. E. Ahmad, H. M. Saleh, and A. F. Hasan, “Automatic semiconductor wafer image segmentation for defect detection using multilevel thresholding,” in *2nd International Conference on Green Design and Manufacture 2016 (ICoGDM 2016)*, 2016, p. 01103. <https://doi.org/10.1051/matecconf/20167801103>
- [16] V. Perminov, V. Putrolaynen, M. Belyaev, E. Pasko, and K. Balashkov, “Automated image analysis for evaluation of wafer backside chipping,” *Int. J. Adv. Manuf. Technol.*, vol. 99, pp. 2015–2023, 2018. <https://doi.org/10.1007/s00170-018-2647-9>
- [17] V. H. Gaidhane, Y. V. Hote, and V. Singh, “An efficient similarity measure approach for PCB surface defect detection,” *Pattern Anal. Appl.*, vol. 21, pp. 277–289, 2018. <https://doi.org/10.1007/s10044-017-0640-9>
- [18] S. Ryu, Y. Sohn, and Y. Yang, “The novel feature based inspection technique that can detect defects that can affect the deterioration of the electrical properties of semiconductor devices,” *Microsc. Microanal.*, vol. 27, no. S1, pp. 792–793, 2021. <https://doi.org/10.1017/S1431927621003147>
- [19] C. Wright and S. J. Yang, “Deep learning for automated focus quality detection in wafer inspection,” in *Automated Visual Inspection and Machine Vision IV*. SPIE, Germany, 2021, pp. 146–157. <https://doi.org/10.1117/12.2592425>

- [20] T. R. Kane and R. A. Levinson, "Formulation of equations of motion for complex spacecraft," *J. Guid. Control*, vol. 3, no. 2, 1980. <https://doi.org/10.2514/3.55956>
- [21] B. Ouyang, Y. H. Liu, H. Y. Tam, and D. Sun, "Design of an interactive control system for a multisection continuum robot," *IEEE/ASME Trans. Mechatron.*, vol. 23, no. 5, pp. 2379–2389, 2018. <https://doi.org/10.1109/TMECH.2018.2855129>
- [22] D. C. Rucker and R. J. Webster III, "Statics and dynamics of continuum robots with general tendon routing and external loading," *IEEE Trans. Robot.*, vol. 27, no. 6, pp. 1033–1044, 2011. <https://doi.org/10.1109/TRO.2011.2160469>